Physics-driven prediction of ab-initio contact area in ionic systems

Marco Di Gennaro[a,*], Szeréna K. Fecske[b,c,d], Konstantinos Gkagkas[e], Carsten Gachot[c], András Vernes[b,d]

[a] *Nanomat, Q-Mat, CESAM, and European Theoretical Spectroscopy Facility, Université de Liège, B-4000 Liège, Belgium*
[b] *Institute of Applied Physics, Technische Universität Wien, Wiedner Hauptstraße 8-10/134, 1040 Vienna, Austria*
[c] *Institute of Engineering Design and Product Development, Technische Universität Wien, Getreidemarkt 9, 1060 Vienna, Austria*
[d] *Austrian Center of Competence for Tribology, AC2T research GmbH, Viktor-Kaplan-Straße 2C, 2700 Wiener Neustadt, Austria*
[e] *Advanced Material Research Division, Toyota Motor Europe NV/SA, Hoge Wei 33B, 1930 Zaventem, Belgium*

Abstract

We present a noise-free numerical method to analytically model and derive interaction forces between ions, based on two detectable and fully distinguishable phase transitions in the *ab-initio* calculated total energies. We use Ionic Liquids as a playground for our numerical scheme with electronic charge densities calculated at MP2-level and atomic separation (contact) area calculated by means of Bader's Quantum Theory of Atoms In Molecules. We show that four different, physics-driven methods give similar results, independently of the system or the approaching direction. Moreover, the so-derived load-dependent separation (contact) area recovers basics physical models, bridging directly the atomistic and the macroscopic length scales.

Keywords: physics-driven modeling, load-dependent *ab-initio* separation (contact) area, multiscale, ionic liquids

1. Introduction

More than fifty-five years ago, with the introduction of the density-functional theory (DFT) [1, 2], a radically novel and revolutionary epoch has been started in both quantum mechanics and computational chemistry. This is furthermore extensively used in the entire community of natural sciences and it was also honoured in 1998 with the Nobel Prize awarded to Walter Kohn for the development of the DFT theory and to John A. Pople for the development of computational quantum chemistry methods [3, 4]. Probably, one of the biggest advantages of DFT is its universality, namely that it is equally well applicable for any realization of matter, from atoms, to molecules up to liquids and solids, *e.g.* , and, additionally, for any of these particular systems at least a couple of highly accurate and available implementations of the DFT exist [5]. With these implementations, one of the central DFT quantities, *i.e.* the electronic (charge) density, minimizing the total energy of the considered system, is also determined in a parameter-free (*ab-initio*) and self-consistent manner [6]. By calculating the gradient of the so obtained electronic density, then one can completely characterize the nanoscopic system of interest from a topological point of view within the Quantum Theory of Atoms in Molecules (QTAIM) by R. F. W. Bader [7, 8, 9].

With this in turn, it opens the opportunity to numerically estimate the separation area between atoms in contact and its dependence on distance [10]. In a way, the present study is a direct continuation of the latter paper by one of the authors, with the main goal of determining the load dependence of the atomic contact area, and it can be seen also as a quantum mechanical foundation of the nanoscopic contact area estimation within classical molecular dynamics (MD) by the same author of the present ones [11].

In spite of the continuously increasing power of computers, however, *ab-initio* calculations still remain expensive for an exhaustive scan of the configuration space and, simultaneously, of the high-dimensional Potential Energy Surface (PES) of a molecule. Therefore, physics-driven modelling of interactions are necessary to avoid imprecise numerical differentiation of the *ab-initio* total energy and still accurately

*Corresponding author.
E-mail address: marco.di.gennaro@external.toyota-europe.com

determine the corresponding interaction forces towards the derivation of the load dependence of the separation area between ions.

In this work, we consider ionic liquids (IL) [12] as model systems for testing our theory. These are composed of organic cations and inorganic anions and exist in liquid phase in a narrow window around room temperature. The combination of different cations and anions allows a huge design potential and to tailor application specific compounds. Indeed, ILs find applications in many different application areas based on their tunable structure and properties: from lubricant additives [13, 14] to green alternatives to traditional solvents [15], to organic catalysis [16] or supercritical fluid applications [17]. ILs are difficult to characterize both from the experimental and from the theoretical point of view [18]. Charge transfer amongst ions was investigated at DFT level leading to contrasting results [19, 20]. These calculations open the door to the centuries old problem concerning the origins of friction. Atomic-scale friction was investigated in an earlier studies[21, 22, 23], where real-contact areas were calculated from electronic contributions on a pure *ab-initio* basis.

The paper is organized as follows: Sec. 2 proposes our novel physics-driven fitting procedure of interaction amongst general ionic systems. The procedure can be applied to non-ionic systems as well. We introduce three different phases and two intermediate phase transitions. We also derive four different methods for the central phase, the one where it makes sense to speak of a non-vanishing contact area between two molecules. Sec. 3 introduces the details of the numerical study and specifics about *ab-initio* calculations, together with data management aspects. In Sec. 4 we report on the results of our strategy and discuss how our derivation agrees both with numerical results and with macroscale models. Sec. 5 contains conclusions and potential outlook. All technical details and convergence study with respect to the *ab-initio* calculations are given in the supplementary information (SI).

2. Physics-driven fitting

Numerical determination of the interaction energy between ions is a demanding task and the determination of forces from numerical values could be very noisy, especially close to structural phase transitions. Therefore, a physics-driven fitting of the total energy to analytical expressions is a solution for accurately determining the interaction forces across different interaction regimes. Since the studied systems here consist of differently charged molecules, long-range Coulomb interactions are present. Additionally, at relatively large distances one should also take into account the van der Waals (vdW) interaction, while at moderate to short distances between the ions a Lennard-Jones (LJ) potential is essential to properly describe the interaction. Thus, in this study, the total energy will be decomposed into these three types of contribution, namely Coulomb, vdW and LJ, exactly in this order.

Since the LJ interaction can be differently parametrized, in the following, four possible sets of LJ parameters will be determined and only the LJ force resulting from the most accurate parametrization with respect to the coefficient of determination R^2 will be then further used.

Considering a nanoscopic system consisting of two distinguishable objects / bodies, *e.g.* , an anion and a cation of an ionic liquid , for which both the total energy $E_{\mathrm{tot}}(r)$ and the separation / contact area $A_{\mathrm{c}}(r)$ have been determined quantum mechanically as a function of the radial distance r between the ions. We can think to r as the distance of the center of masses of the two components. To obtain the load-dependent contact area $A_{\mathrm{c}}(L)$ between ions (which is in practice a much more pragmatic and widely used quantity), one has to calculate the load:

$$L = -\frac{dE_{\mathrm{tot}}(r)}{dr} \ . \tag{1}$$

An accurate numerical differentiation of $E_{\mathrm{tot}}(r)$ would require the knowledge of the total energy for a large amount of radial positions. From a computational point view, it is much more efficient to first fit $E_{\mathrm{tot}}(r)$ – using its value at a modest number of radial distances – to an analytically provided model function, which has to be set, based on the physics happening within the nanoscopic system, and then to apply Eq. (1) for obtaining analytically the load L.

For this, we proceed as follows. Observing that three physically different interaction regions can be distinguished, two characteristic transition distances can be introduced. In the large r phase, or *separable* phase, the two bodies are far away from each other and hence totally separable. The contact surface is zero. As the bodies approaches each other, the separation radius reaches a value where the two bodies are

no longer separable, though they are still distinguishable from one another. We dub this value the jump-to-contact (j2c) distance or d_{j2c} . This corresponds to the point where the contact area $A_{\mathrm{c}}(r)$ between the ions, which is the order parameter of the transition, is not vanishing for the first time. We define this the *distinguishable* phase, and this is the phase where our derivation is more significant. The ionic charge of the two ions remains close to $\pm e$, with e being the elementary charge of a single electron. As the ions move further close to one another, a second phase transition occurs at a radial distance defined as jump-to-merge (j2m) or d_{j2m} , below which the two objects cannot be distinguished and are merged into a single body, or into an *indistinguishable* phase. In this phase, it makes no longer sense to speak of two different objects, their ionic charges strongly differ from $\pm e$. Loads corresponding to total energies at radial distances within $(0,\, d_{\mathrm{j2m}}] \subset \mathbb{R}_+$ will be completely omitted from our discussion, since within the *indistinguishable* domain, the separation area between them (our major interest in the present work) is not defined.

With all these in mind, it becomes clear that the total energy of the system minus the energies of the isolated objects, which in the case of an IL corresponds to the interaction energy between the ions, has at least three components, namely the Coulomb energy due to the charges of involved ions, the long-range van der Waals energy, and a remaining part for which a plausible physical approach has to be made, *e.g.* to be Lennard-Jones type. This latter part of the energy is more important in the *distinguishable* phase and is the central part of this study, because it models the domain where the separation area between the objects, say ions, is of finite, non-zero value.

2.1. Elimination of the van der Waals background

In a first step, one extracts from the total energy of the system $E_{\mathrm{tot}}(r)$, the long-range Coulomb interaction energy $E_{\mathrm{C}}(r)$ and calculates:

$$E_{\mathrm{nC}}(r) = E_{\mathrm{tot}}(r) - E_{\mathrm{C}}(r) \ , \qquad \forall r \in \mathbb{R}_+ \tag{2}$$

where:

$$E_{\mathrm{C}}(r) = \frac{1}{4\pi\epsilon_0}\frac{q_{\mathrm{a}}\, q_{\mathrm{c}}}{r} \ , \tag{3}$$

with q_{a} and q_{c} being the total charges of the ions as obtained by integrating the quantum mechanically calculated charge densities. Note that the Coulomb force derived from Eq. (3),

$$F_{\mathrm{C}}(r) = -\frac{dE_{\mathrm{C}}(r)}{dr} = \frac{1}{4\pi\epsilon_0}\frac{q_{\mathrm{a}}\, q_{\mathrm{c}}}{r^2} \tag{4}$$

is a constitutive part of the load L introduced in Eq. (1). Now, the remaining part of the total energy $E_{\mathrm{nC}}(r)$ has to be separately modelled in accordance with the undergoing physics in three phases of the radial distance r.

Quite obviously, for large radial distances $r > d_{\mathrm{j2c}}$, the nanoscopic system should behave like a purely vdW system, *i.e.* , the non-Coulomb part of the total energy and the relative derived force $\forall r \in [d_{\mathrm{j2c}},\, +\infty)$ are given by:

$$E_{\mathrm{vdW}}(r) = \frac{C_{\mathrm{vdW}}}{r^6} \ , \qquad \forall r \in [d_{\mathrm{j2c}},\, +\infty) \tag{5}$$

and

$$F_{\mathrm{vdW}}(r) = -\frac{dE_{\mathrm{vdW}}(r)}{dr} = \frac{6}{r^7}\, C_{\mathrm{vdW}} \ . \tag{6}$$

To evaluate $C_{\mathrm{vdW}} \in \mathbb{R}$, supposing that the non-Coulomb part of the total energy in Eq. (2) is known at the radial positions $r_i \in [d_{\mathrm{j2c}},\, +\infty)$ where $i = 1, \ldots, N_{\mathrm{vdW}}$, namely $E_{\mathrm{nC}}(r_i) \equiv E_i^{(\mathrm{nC})}$. Let us impose that C_{vdW} minimizes the chi-square merit function of unity weights set for the model vdW function from Eq. (5),

$$\chi^2\left(C_{\mathrm{vdW}}\right) = \sum_{i=1}^{N_{\mathrm{vdW}}} \left[E_{\mathrm{nC}}(r_i) - E_{\mathrm{vdW}}(r_i)\right]^2 = \sum_{i=1}^{N_{\mathrm{vdW}}} \left(E_i^{(\mathrm{nC})} - \frac{C_{\mathrm{vdW}}}{r_i^6}\right)^2 \tag{7}$$

and hence:

$$C_{\mathrm{vdW}} = \frac{\displaystyle\sum_{i=1}^{N_{\mathrm{vdW}}} \frac{E_i^{(\mathrm{nC})}}{r_i^6}}{\displaystyle\sum_{i=1}^{N_{\mathrm{vdW}}} \frac{1}{r_i^{12}}} \ . \tag{8}$$

Thus, the elimination of the vdW background from the non-Coulombic part of the interaction energy is achieved by considering

$$E_{nC-\mathrm{vdW}}(r) = E_{\mathrm{nC}}(r) - E_{\mathrm{vdW}}(d_{\mathrm{j2c}}) \equiv E(r) \ , \qquad \text{for} \quad \forall r \in (d_{\mathrm{j2m}},\, d_{\mathrm{j2c}}] \ . \tag{9}$$

Note that in Eq. (9) we choose a constant shift $E_{\mathrm{vdW}}(d_{\mathrm{j2c}}) = \text{const.}$ and not a radial-dependent value for $E_{\mathrm{vdW}}(r)$ as introduced in Eq. (5) for the reason becoming clear in the immediate next section. Moreover, if $|E_{\mathrm{nC}}(d_{\mathrm{j2c}}) - E_{\mathrm{vdW}}(d_{\mathrm{j2c}})|$ is relatively large, *i.e.* , the quantum mechanically calculated non-Coulomb part of the total energy at the jump-to-contact $E_{\mathrm{nC}}(d_{\mathrm{j2c}})$ visibly differs from the value of the model vdW function at the same place $E_{\mathrm{vdW}}(d_{\mathrm{j2c}})$, then one could use $\min\left[E_{\mathrm{nC}}(d_{\mathrm{j2c}}),\, E_{\mathrm{vdW}}(d_{\mathrm{j2c}})\right]$ for the constant energy-shift in Eq. (9).

2.2. Lennard-Jones fitting

In the following, $E(r)$ defined in Eq. (9) is fitted to the generalized m-n Lennard-Jones potential:

$$E_{\mathrm{LJ}}^{(m\neq n)}(r) = \frac{E_0}{m-n}\left[m\left(\frac{d_0}{r}\right)^n - n\left(\frac{d_0}{r}\right)^m\right] \ , \qquad m,n \in \mathbb{N}_+ \ . \tag{10}$$

Accordingly, if the initial vdW character of the nanoscopic system persists also when $r \in (d_{\mathrm{mtl}},\, d_{\mathrm{j2c}}]$, then it will show up in the results of the m-n LJ fitting too. Otherwise, the system changes its character from a purely vdW to a LJ one (which has no vdW part), *i.e.* the *separable* to *distinguishable* phase transition is occurring. The corresponding force:

$$F_{\mathrm{LJ}}^{(m\neq n)}(r) = -\frac{dE_{\mathrm{LJ}}^{(m\neq n)}(r)}{dr} = \frac{mn}{m-n}\,\frac{E_0}{d_0}\left[\left(\frac{d_0}{r}\right)^{n+1} - \left(\frac{d_0}{r}\right)^{m+1}\right] \tag{11}$$

vanishes for $r = d_0$, which is the equilibrium distance within the nanoscopic system with E_0 being the depth of the potential well.

Similarly to the elimination of the vdW background, knowing $E(r_i) \equiv E_i$ in Eq. (9) for a finite number of radial distances in the *distinguishable* phase $r_i \in (d_{\mathrm{mtl}},\, d_{\mathrm{j2c}}]$, where $i = 1, \ldots, N_{\mathrm{LJ}}$, and for a given pair of natural numbers m and n, we introduce the chi-square merit function to be minimized in order to get the best (m, n) combination:

$$\chi^2_{m,n} = \sum_{i=1}^{N_{\mathrm{LJ}}}\left[E(r_i) - E_{\mathrm{LJ}}^{(m\neq n)}(r_i)\right]^2 \tag{12}$$

With this in mind, both real-valued parameters E_0 and d_0 in Eq. (10) can be easily derived, and one could straightforwardly obtain m and n by properly applying a non-linear fitting scheme.

Alternatively, one can rewrite Eq. (10) as follows:

$$E_{\mathrm{LJ}}^{(m\neq n)}(r) = \frac{A_{\mathrm{LJ}}}{r^n} - \frac{B_{\mathrm{LJ}}}{r^m} \ , \qquad \text{with} \quad A_{\mathrm{LJ}}, B_{\mathrm{LJ}} \in \mathbb{R} \ . \tag{13}$$

Indeed, also the parameters A_{LJ} and B_{LJ} are determined by imposing that they minimize the appropriate chi-square merit function of unity weights, namely:

$$\chi^2_{m,n}\left(A_{\mathrm{LJ}}, B_{\mathrm{LJ}}\right) = \sum_{i=1}^{N_{\mathrm{LJ}}}\left[E(r_i) - E_{\mathrm{LJ}}^{(m\neq n)}(r_i)\right]^2 = \sum_{i=1}^{N_{\mathrm{LJ}}}\left(E_i - \frac{A_{\mathrm{LJ}}}{r_i^n} + \frac{B_{\mathrm{LJ}}}{r_i^m}\right)^2 \ . \tag{14}$$

In this manner, one immediately obtains:

$$\left\{\begin{array}{rcl} A_{\mathrm{LJ}} & = & \dfrac{S_1 S_{22} - S_2 S_{12}}{\Delta} \\ \\ B_{\mathrm{LJ}} & = & \dfrac{S_2 S_{11} - S_1 S_{21}}{\Delta} \end{array}\right. \ , \qquad \text{with} \quad \Delta = S_{11}S_{22} - S_{12}S_{21} \ , \tag{15}$$

where involved summations are:

$$\left\{\begin{array}{rcl} S_{11} &=& +\displaystyle\sum_{i=1}^{N_{\mathrm{vdW}}} \frac{1}{r_i^{2n}} \\ \\ S_{22} &=& -\displaystyle\sum_{i=1}^{N_{\mathrm{vdW}}} \frac{1}{r_i^{2m}} \end{array}\right. , \qquad S_{12} = -\sum_{i=1}^{N_{\mathrm{vdW}}} \frac{1}{r_i^{m+n}} = -S_{21} \qquad \text{and} \qquad \left\{\begin{array}{rcl} S_1 &=& \displaystyle\sum_{i=1}^{N_{\mathrm{vdW}}} \frac{E_i}{r_i^n} \\ \\ S_2 &=& \displaystyle\sum_{i=1}^{N_{\mathrm{vdW}}} \frac{E_i}{r_i^m} \end{array}\right. . \tag{16}$$

It is also shown that the so estimated fitting parameters A_{LJ} and B_{LJ} have the accuracy as specified by the squared standard deviations and covariances:

$$\left\{\begin{array}{rcl} \sigma^2_{A_{\mathrm{LJ}}} &=& \dfrac{S_{22}}{\Delta} \\ \\ \sigma^2_{B_{\mathrm{LJ}}} &=& \dfrac{S_{11}}{\Delta} \end{array}\right. \qquad \text{and} \qquad \left\{\begin{array}{rcl} c_{A_{\mathrm{LJ}},B_{\mathrm{LJ}}} &=& -\dfrac{S_{12}}{\Delta} \\ \\ c_{B_{\mathrm{LJ}},A_{\mathrm{LJ}}} &=& -\dfrac{S_{21}}{\Delta} \end{array}\right. . \tag{17}$$

Accordingly, the proposed m-n LJ fitting scheme consists the following steps:

- calculation of A_{LJ} and B_{LJ} using Eqs. (15) and (16) together with the corresponding goodness-of-fit $\chi^2_{m,n}\left(A_{\mathrm{LJ}}, B_{\mathrm{LJ}}\right)$, recall Eq. (14), the absolute errors $\sigma_{A_{\mathrm{LJ}}}$ and $\sigma_{B_{\mathrm{LJ}}}$ as square root of variances and the covariance $c_{A_{\mathrm{LJ}},B_{\mathrm{LJ}}} = -c_{B_{\mathrm{LJ}},A_{\mathrm{LJ}}}$, see Eq. (17), for all pairs $(m,n) \in \mathbb{N}^2_+$ of interest, for example, for $m,\, n = 1, 2, \ldots, 20$ $(m \neq n)$;
- selection of m and n as those which produce the smallest $\chi^2_{m,n}\left(A_{\mathrm{LJ}}, B_{\mathrm{LJ}}\right)$, then fix $A_{\mathrm{LJ}} \pm \sigma_{A_{\mathrm{LJ}}}$ and $B_{\mathrm{LJ}} \pm \sigma_{B_{\mathrm{LJ}}}$ for the LJ contribution to the load

$$F_{\mathrm{LJ}}^{(m\neq n)}(r) = n\,\frac{A_{\mathrm{LJ}}}{r^{n+1}} - m\,\frac{B_{\mathrm{LJ}}}{r^{m+1}} \tag{18}$$

- finally, one should also verify how accurately provides

$$d_0 = \left(\frac{n}{m}\frac{A_{\mathrm{LJ}}}{B_{\mathrm{LJ}}}\right)^{\dfrac{1}{n-m}} \tag{19}$$

the equilibrium distance of the two constitutive objects bodies and

$$E_0 = \frac{m-n}{m} A_{\mathrm{LJ}}\, d_0^{-n} = \frac{m-n}{n} B_{\mathrm{LJ}}\, d_0^{-m} \tag{20}$$

the energy minimum of the nanoscopic system.

Recall that loads corresponding to the total energies at radial distances in $(0,\, d_{\mathrm{mtl}}] \subset \mathbb{R}_+$ are completely omitted from our discussion because within this domain, the two initially separate objects / bodies cannot be distinguished and hence the separation / contact area between them (our major interest in the present work) is not defined / available.

Lastly, when $m = n$, Eq. (10) can be rewritten as:

$$\begin{aligned} E_{\mathrm{LJ}}^{(m=n)}(r) &= \lim_{n\to m} E_{\mathrm{LJ}}^{(m\neq n)}(r) \\ &= E_0\left[1 - n\ln\left(\frac{d_0}{r}\right)\right]\left(\frac{d_0}{r}\right)^n \\ &= \frac{a_{\mathrm{LJ}}}{r^n} - b_{\mathrm{LJ}}\frac{\ln r}{r^n}, \qquad\qquad \text{with} \quad a_{\mathrm{LJ}}, b_{\mathrm{LJ}} \in \mathbb{R} \end{aligned} \tag{21}$$

such that:

$$a_{\mathrm{LJ}} = E_0(1 - n\ln d_0)d_0^n \tag{22}$$

$$b_{\mathrm{LJ}} = -nE_0 d_0^n\ , \tag{23}$$

or alternatively:

$$d_0 = \exp\left(\frac{1}{n} + \frac{a_{\rm LJ}}{b_{\rm LJ}}\right) \tag{24}$$

$$E_0 = -\frac{b_{\rm LJ}}{n}\exp\left[-\left(1 + n\frac{a_{\rm LJ}}{b_{\rm LJ}}\right)\right] \tag{25}$$

and accordingly:

$$\begin{aligned} F_{\rm LJ}^{(m=n)}(r) =& -\frac{dE_{\rm LJ}^{(m=n)}(r)}{dr} \\ =& -n^2 E_0 \ln\left(\frac{d_0}{r}\right)\frac{d_0^n}{r^{n+1}} \\ =& n\,\frac{a_{\rm LJ}}{r^{n+1}} + \frac{b_{\rm LJ}}{r^{n+1}}\left(1 - n\ln r\right) \ . \end{aligned} \tag{26}$$

Similarly to the previous case of $m \neq n$, having $E(r_i) \equiv E_i$ in Eq. (9) for a finite number of radial distances $r_i \in (d_{\rm mtl},\, d_{\rm j2c}]$, where $i = 1, \ldots, N_{\rm LJ}$, now, for a given value of $m = n$, the parameters $a_{\rm LJ}$ and $b_{\rm LJ}$ are directly resulting from the minimization of the following chi-square merit function with unity weights:

$$\chi^2_{m=n}\left(a_{\rm LJ}, b_{\rm LJ}\right) = \sum_{i=1}^{N_{\rm LJ}}\left[E(r_i) - E_{\rm LJ}^{(m=n)}(r_i)\right]^2 = \sum_{i=1}^{N_{\rm LJ}}\left(E_i - \frac{a_{\rm LJ}}{r_i^n} + b_{\rm LJ}\frac{\ln r_i}{r_i^n}\right)^2 \ , \tag{27}$$

i.e. :

$$\left\{\begin{array}{lcl} a_{\rm LJ} &=& \dfrac{S_1 s_{22} - s_2 s_{12}}{\delta} \\ \\ b_{\rm LJ} &=& \dfrac{s_2 s_{11} - S_1 s_{21}}{\delta} \end{array}\right. \quad , \qquad \text{with} \quad \delta = S_{11}s_{22} - s_{12}s_{21} \ , \tag{28}$$

where S_{11} and S_1 are as introduced in Eq. (16):

$$s_{22} = -\sum_{i=1}^{N_{\rm LJ}}\frac{\ln^2 r_i}{r_i^{2n}} \ , \qquad s_{12} = -\sum_{i=1}^{N_{\rm LJ}}\frac{\ln r_i}{r_i^{2n}} = -s_{21} \qquad \text{and} \qquad s_2 = \sum_{i=1}^{N_{\rm LJ}} E_i\frac{\ln r_i}{r_i^n} \ . \tag{29}$$

Finally, the accuracy of the so obtained fitting parameters $a_{\rm LJ}$ and $b_{\rm LJ}$ is given by the squared standard deviations and covariances:

$$\left\{\begin{array}{lcl} \sigma^2_{a_{\rm LJ}} &=& \dfrac{s_{22}}{\delta} \\ \\ \sigma^2_{b_{\rm LJ}} &=& \dfrac{S_{11}}{\delta} \end{array}\right. \qquad \text{and} \qquad \left\{\begin{array}{lcl} c_{a_{\rm LJ},b_{\rm LJ}} &=& -\dfrac{s_{12}}{\delta} \\ \\ c_{b_{\rm LJ},a_{\rm LJ}} &=& -\dfrac{s_{21}}{\delta} \end{array}\right. \ . \tag{30}$$

In view of all these possibilities, one can follow four different LJ fitting strategies and compare them in their accuracy, see Tab. 1.

LJ1: E_0 and d_0 in Eq. (10) are set to the lowest interaction energy and corresponding radial distance between ions from numerical calculations. The pair of exponents (m, n) is then determined to be the one which minimizes the corresponding merit function $\chi^2_{m,n}$ in Eq. (12) and/or maximizes the relativ coefficient of determination R^2.

LJ2: Differs from the previous LJ1-strategy in only that both E_0 and d_0 are also varied on a grid around their *ab-initio* obtained values, until $\chi^2_{m,n}(E_0, d_0)$ reaches its minimum for every pair of (m, n) separately. At the end then one gets that combination of E_0, d_0, m and n for which the merit function $\chi^2_{m,n}(E_0, d_0)$ achieves its overall lowest value. Precisely, we uniformly varied d_0 and E_0 on an grid of 20x20 values in the range of ± 1Å and ± 0.5 Ha around the numerical values corresponding to the energy well minimum.

LJ3: This is the implementation of the LJ parametrization from Eq. (13) along with Eqs. (14) – (16) and Eq. (17), which yields A_{LJ} and B_{LJ} for that pair of (m, n) which provides the lowest possible minimum of $\chi^2_{m,n}(A_{LJ}, B_{LJ})$ Eq. (14).

LJ4: It is the counterpart of LJ3 for $m = n$, recall Eq. (21), and using Eqs. (27) – (30).

3. Computational details

3.1. Configurations

For the purpose of this study, two ionic liquids were considered, namely 1-Ethyl-3-methylimidazolium tetrafluoroborate (EMIM-BF_4) and 1-Ethyl-3-methylimidazolium hexafluorophosphate (EMIM-PF_6), see Fig. 2. These ILs consist of the same cation (EMIM) and a different anion (BF_4 or PF_6) respectively. The cation consists of a five-membered imidazole derivate ring with two nitrogen and three carbon atoms, with an ethyl and methyl groups connected at the two nitrogen atoms. The geometry of the anions is symmetrical, therefore reducing the number of degrees of freedom and thus the complexity of this study. On the other hand, the cation has a quasi-planar geometry and therefore interacts on a different way with the anion, depending on the approach direction.

For a complete characterisation of their interaction energies, a three-dimensional Potential Energy Surface needs to be calculated. A geometrical constraint was imposed to reduce the number of variables on the Potential Energy Surface (PES) from $3*N$ to 3, with N being the number of atoms. For the representation of the different configurations in a three-dimensional space, a polar coordinate system was implemented. For the cation, the reference system was set according to the C atom in between the two N atoms in the imidazole ring (C_1), the C atom closer to the ethyl chain (C_2), the N atom between C_1 and C_2. For the anion the central atom, *i.e.* B and P for BF_4 and PF_6 respectively, were taken as reference. The distance between C_1 and the central anion atom was evaluated as the radial distance between the ions. This distance is equivalent to the distance between center of masses of the two ions in the *separable* phase, while these two diverge in the *distinguishable* phase. We finally selected the latter over the former as it led to a reduction of numerical noise. The azimuth angle Θ was defined as the angle between C_1-C_2 and the central anion atom and the longitudinal angle Φ was set equal to the dihedral angle between C_1-C_2-N and the central anion atom. This triplet of spherical coordinates (r, Θ, Φ) is representing a single point in the PES. Note that the coordinate values were constrained in our calculations while the positions of all the other atoms in the molecules were relaxed. The full PES is shown in the SI. Here we show only results for two selected directions, representing the relative positions on opposing sides of the y-axis. This means that the system was analyzed here only when the anion is approaching the cation either from the -y direction or from the +y direction.

3.2. Ab-initio calculations

All *ab-initio* calculations in this study were performed with GAMESS (US) [24, 25]. All considered systems were simulated in the gas phase, within a restricted Hartree-Fock closed-shell, fully occupied, scheme. Structural optimization was carried out within DFT with the Pople's "triple split" and 6 Gaussian $6-311{+}G^{**}$ basis set [26, 27, 28, 29] and the B3LYP functional [30, 31, 32, 33]. More details as well as a convergence study are presented in the SI. The gradient convergence tolerance was set to 10^{-4} Hartree/Bohr. The Grimme's empirical DFT-D3(BJ) dispersion correction involving scaled vdW terms was used [34]. Total energies were calculated on top of DFT optimized geometries within the Møller–Plesset perturbation theory at the second order (MP2).

The manifolds representing the atoms and molecules were obtained by partitioning the charge density according to Bader's QTAIM. Within QTAIM, each atomic manifold is represented by a 3D object centered around the nuclei. This atomic basin is bounded by the so-called inter-atomic surface (IAS) which is of "zero-flux" for the electronic charge density and could take up any convex shape [35]. Therefore, the calculation of any atomic properties is performed by integration over the corresponding atomic basin. The so resulting atomic properties are highly dependent on the accuracy of the basin integration method and by the choice of the basin quadrature. Accordingly, all calculations were set here to achieve a high numerical accuracy by increasing the maximum atomic integration radius (set to 20 a.u.), the basin quadrature points (set to "Sky High") and the fineness of the IAS mesh (set to "Very Fine").

Having the topological partitioning of the molecules into atoms, the separation area between the anion and the cation is defined as the sum of the inter-atomic surfaces between the atoms which belong to the anion (BF_4 or PF_6) and the cation (EMIM).

Computationally, the Atoms in Molecules (AIM) analysis of the ionic systems was realized by using the AIMALL software package [36]. The wavefunctions of the ionic systems resulting from MP2 calculations were directly used as input for AIM analysis. This topological analysis of the electronic charge density performed with AIMALL provides the following properties of our interest: the Bader charges calculated for each atom, their volumes and surface area, and the inter-atomic surface areas between all pairs of atoms connected by a bond-path.

3.3. Data management

In order to handle and manage the data flow and the numerical calculations, a database was built to track and couple the computational results obtained with GAMESS and AIMALL. On top of these, a Python interface was implemented, which includes the numerical methods described in the theoretical part, *e.g.* , to analyze the various type of interactions within the ionic system.

We used a sqlight3 relational database built using DJANGO [37] – a high-level Python Web framework. Within this framework, one can use Django to build the database and integrate it in the Python scripts used for post-processing of data. In addition, since numerical calculations are prone to convergence errors and are very sensitive to the choice of some input parameters, the database is also storing the relevant metadata of each run. More information is given in the SI.

4. Load-dependent separation area between ions

In this section, we are reporting the numerical results in Tabs. 1 and 2, as obtained by using our physics-driven fitting method from Sec. 2, in order to deduce the functional dependence of the separation area $A_{\mathrm{c}}(r)$ on the interaction force (or load) between the ions. This modeling strategy is primarily motivated by the fact that *ab-initio* calculations are quite expensive for a numerically accurate determination of the load without any supplementary hypothesis and they can be very noisy. Indeed, by inspecting Fig. 1, where the *ab-initio* total energies for the two considered ionic systems are compared with the corresponding forces directly calculated by numerical differentiation (the NUMPY.GRADIENT() method was used), it becomes obvious that these forces are too noisy and with a strong tendency for oscillations. Thus, numerical differentiation of the *ab-initio* total energy is an unreliable scheme for extracting the underlying physical mechanisms, as well as for the up-scaling of the forces to be used in molecular dynamics simulations, for example. In this Fig. 1 and in all the following ones, red and blue (colors online) refer to EMIM-BF_4 and EMIM-PF_6 , respectively, while triangles are oriented in accordance with the approaching direction of the two ions, namely +y or −y, as described in Sec. 3.1.

In view of all these, it is not a surprise that in Fig. 5, where the total interaction energy is decomposed into its Coulomb and non-Coulomb parts, one can also clearly identify the two distances d_{j2m} and d_{j2c} of ionic phase transitions, see vertical dotted lines. The Coulomb part of the total energies was determined by using the Bader charges from our QTAIM analysis, which in turn was performed for wavefunctions resulting from MP2 calculations. Unfortunately, Mulliken charges are strongly basis-dependent quantities and yield spurious charge transfers which are not known to happen - more details are given in the SI. In contrast to Mulliken charges, in Fig. 5 it can be seen that the Bader charge of the anion and cation remains constant within a window of $\pm$ 0.03e (with e being the elementary charge) around -1e and 1e, respectively, exactly as known from chemistry textbooks, and this until the distance between the ions reaches values close to d_{j2m} where it approaches $\pm$ 0.1e. An even more pronounced change of the charge values is then observed as the ions further approach each other in the *indistinguishable phase*. This can be potentially attributed to numerical inaccuracies in the AIM-analysis, as well as the ill defined notion of distinguishable ions at very small distances. Furthermore, Fig. 5 is also confirming that the Coulomb interaction is dominant for ionic systems. At the same time, it should be noted that our methodology is equally applicable to non-ionic systems too by skipping this first step of decomposition of the total energy.

Dealing with non-overlapping Bader manifolds above d_{j2c} , the systems energetically are turning from ionic into molecular ones after the subtraction of the Coulomb contribution, *i.e.* , at large separation distances when $r > d_{\mathrm{j2c}}$, the interacting molecules should behave as purely van der Waals particles. Therefore, in a next step, we eliminate the van der Waals background from the non-Coulomb part of the total energy by closely following the procedure given in Eqs. (5) - (8). This does not mean that the vdW contribution could not persist below d_{j2c} too, but that its eventual further existence within the *distinguishable* phase too has to be confirmed separately. For this, one has to consider the four Lennard-Jones fitting schemes provided in Sec. 2.2, and look in Tab. 1 for the occurrence of $m = 6$ and/or $n = 6$, *e.g.* , LJ3 lines while approaching of ions along +y in both systems. Before starting the LJ-fittings, however, one is shifting the non-Coulomb part of the total energy $E_{\mathrm{nC}}(r)$ to zero at d_{j2c} by means of Eq.(9), namely by subtracting the constant value of $E_{\mathrm{vdW}}(d_{\mathrm{j2c}})$ from this. It can be also observed that an extrapolation of $E_{\mathrm{nC-vdW}}(r) \equiv E(r)$ beyond d_{j2c} by using the fitting parameters from Tab. 1, yields negligible values for $r > d_{\mathrm{j2c}}$, confirming once again that the molecules at large separation distances are predominantly of vdW character - as shown also in Fig. 6.

In Fig. 6 all obtained m-n LJ potentials are plotted for $r > 0$ by fitting $E(r) = E_{\mathrm{nC-vdW}}(r)$ in Eq. (9) with $r \in (d_{\mathrm{mtl}}, d_{\mathrm{j2c}}] \subset \mathbb{R}_+$ to the forms given in Eqs.(10), (13) and (21), recall Tab. 1. The results listed in Tab. 1, *e.g.* , m and n which are also included in the legend of Fig. 6, are all providing the highest coefficients of determination R^2. For sake of completeness, in this Tab. 1 it is also given the value of merit function, as another measure for the goodness of fit, *i.e.* χ^2 as introduced in Eqs.(12), (14) and (27) for the numerically determined fitting parameters using *ab-initio* MP2-results. Interestingly, independently of the type of the EMIM-based IL, the best LJ-potentials are those which have $m = 7$ and $n = 8$ for the approaching along the negative y-axis, and $m = 5$ and $n = 6$ (*i.e.* , with a surviving vdW interaction) for the approaching of ions along the positive y-axis, thus within the region of non-vanishing separation area, the interaction between the ions is only depending on their relative orientation. Note that only combinations of exponents 5, 6 and 7 are typically found for ILs in the literature by fitting $E_{\mathrm{nC}}(r)$ without removing the vdW background. [38] In addition, previous molecular dynamics studies of model ILs represented by coarse-grained particles have typically employed exponents of 12 and 6 [39, 40, 41, 42]. Going beyond the exponent values, our fitting procedure also produces the equilibrium distance d_0 and minimum energy E_0 of the nanoscopic system. Previous coarse grained studies [39, 40] have applied a comparable equilibrium distance of 8.4 Å, however the minimum interaction energies were weaker by more that 3 orders of magnitude compared to real ion pairs. Such a discrepancy was necessary for obtaining a liquid phase at room temperature conditions as the coarse-grained geometry of the ions in combination with point charges strongly promotes crystallisation compared to real ILs. Nevertheless, out fitting method can provide insights for the development of coarse-grained models that can represent actual ILs at a reduced computational cost.

Also interesting in Tab. 1 is that $m = n = 5$, 6, 7 and 8 provided by the LJ4-fitting have the same R^2 as those for the LJ3 fitting, and these single terms are not necessarily those which are dominating the $m \neq n$ cases. This means, that it is also possible to suppress one LJ-type interaction by taking the limit of $m = n$, and the term which is persisting to exist is that one, which describes mostly the leading interaction and its physics. Furthermore, the exponent of this particular $m = n$ LJ-potential could allow one also to distinguish between ions and their relative orientation.

Nevertheless, in the following, the parameters of $m \neq n$ LJ3 fitting will be used to separately access both the repulsive and attractive parts of the interaction potential, and accordingly also in Eqs.(11), (18) and (26) for the computation of the LJ-forces. Since the so modelled energy well matches the ab-initio total energy as shown in Fig. 7a, our methodology suffices for reproducing the main features of the potential energy surface in case of ionic systems. Furthermore, the forces analytically resulting from these energies, see Fig. 7b, are significantly smoother in their radial dependence than the numerically derived ones n Fig. 1 with a single slight discontinuity at d_{j2c} . Therefore, these forces can now be used to determine the load dependence of the separation area between the ions.

The separation area A between the ions is determined based on Bader's QTAIM for the same set of radial distances for which the *ab-initio* total energies were calculated, see Fig. 8a (left panel), and on a first glance seems to vary almost linearly with the distance between the ions. Knowing also the interaction force (load) L between the ions on the same radial grid by analytically differentiating the *ab-initio* total energy fitted to various functional dependencies, like vdW and LJ, the load-dependence of the separation area $A(L) \equiv A$ immediately results as shown in Fig. 8a (right panel). By closely inspecting the load dependence of the separation area, recall the inset in Fig. 8a (right panel), it becomes immediately evident the similarity of our *ab-initio* $A(L)$ with the load-dependence of the real contact area within the macroscopic adhesive contact model by Johnson, Kendall and Roberts (JKR) [43, 44]. In some extent, this could be expected, since the validity of the JKR-model on the nanoscale was experimentally proven by measuring the friction force against the load in an atomic force microscope (AFM) [45], and applying the Bowden-Tabor kinetic friction law to relate the friction force to the load-dependent contact area - shown also to be valid at nanoscale in dry sliding conditions [46, 47]. What is surprising, however, is that exactly the JKR-model seems to formally describe also for the load dependence of the *ab-initio* separation area between the ions. Indeed, considering the load L_0 in the vicinity of d_{j2c} , where $A(L_0) \equiv A_0$ has a tiny non-vanishing positive value, as reference, the left panels of Fig. 8b directly confirms that

$$\ln \frac{A}{A_0} = \gamma + \beta \, \ln \frac{L}{L_0} \ . \tag{31}$$

Namely, that the separation area between the ions follows a power-law dependence on the load, *i.e.* ,

$$A(L) = \alpha \, L^{\beta} \ , \qquad \text{with} \quad \alpha = \frac{A_0 \, e^{\gamma}}{L_0^{\beta}} \ , \tag{32}$$

where $\beta = 1\,/\,10$ with $R^2 > 93$ and 74 % for EMIM-BF_4 and EMIM-PF_6 , respectively, recall Tab. 2. In contrast to the universality of β, the prefactor α in Eq. (32), see its value in Tab. 2, is distinguishing between the ILs and direction of approaching, respectively. Having this common value of the exponent β different than $2\,/\,3$, it is again a clear evidence for the non-Hertzian character of the contact between the ionic Bader manifolds. Unfortunately, the confirmed JKR-contact between ions forming ILs gives no hints on the upscaling, namely how the load dependence of the total *ab-initio* separation area for an ensemble of ions could be.

5. Summary and Conclusions

This research paper highlighted a noise-free numerical method to analytically model and derive interaction forces between ions. The numerical determination of the interaction energy between ions is usually quite challenging and the resulting numerical noise close to relevant points such as the jump to contact of the two molecules hinders the proper calculation of the respective forces. The strategy in this research paper was to decompose the interaction energy in three major contributions namely the Coulomb-, the van der Waals- and Lennard-Jones interaction and to apply a physics-driven fitting procedure of the total energy to analytical formulae to finally calculate the forces. For this we used two ionic liquids EMIM-BF4 and EMIM-PF6 as model sytems. The following conclusions can be drawn:

- The presented approach can filter out the numerical noise from the data and allows for a quantified and fundamental study of the interaction forces in ionic systems. However, the approach can be also transferred to non-ionic system if the first step of the decomposition of the total energy is skipped.
- The shown procedure clearly highlights the existence of a universal behaviour independent of the system studied, the directions and fitting method. In this particular case, independent of the EMIM-based ionic liquid, the Lennard-Jones potential results in coefficients m = 7 and n = 8 along the negative y-axis and additionally m = 5 as well n = 6 along the positive y-axis. This actually means that within the region of non-vanishing separation area, the interaction between the ions of the ionic liquids only depend on their relative orientation.
- The load dependent ab-initio separation area A(L) has significant similarities with the load dependence of the real contact area within the macroscopic adhesive contact model by Johnson, Kendall and Roberts (JKR model). Interestingly, the JKR model seems to properly describe also the load dependence of the ab-initio separation between the ions thus connecting the macroscopic world with the atomistic level.

These calculations shed some light onto the centuries old problems concerning the origins of friction and the research presented may contribute to a better understanding for the design of additive molecules and therefore improvements in the operation and longevity of machine elements as a future outlook.

6. Acknowledgements

MDG acknowledges Klanik SA.

This work was funded by the "Austrian COMET-Program" (project: InTribology, no. 872176) via Austrian Research Promotion Agency (FFG) and the federal States of Niederösterreich and Vorarlberg, and it has been carried out within the "Excellence Centre of Tribology" (AC2T research GmbH).The government of Lower Austria is gratefully acknowledged for financially supporting the endowed professorship tribology of Prof.Dr. C. Gachot at the TU Wien (Grant No. WST3-F 5031370/001-2017) in collaboration with AC2T research GmbH.

System	***dir.***	$d_0^{num.}(Å)$	$E_0^{num.}(Ha)$	$d_{\mathrm{j2m}}(Å)$	$d_{\mathrm{j2c}}(Å)$	$E_{vdW}^{d_{\mathrm{j2c}}}(Ha)$	C_{vdW} *10^{-4}	χ^2_{vdW}	*Fit*	m	n	χ^2	R^2	$d_0(Å)$	$E_0(Ha)$
EMIM-BF_4	-y	4.971	-0.221	3.795	6.707	-0.195	-1.777	0.008	LJ1	6	8	0.088	0.963		
									LJ2	5	9	0.065	0.972	5.024	-0.195
									LJ3	7	8	0.054	0.977	4.957	-0.172
									LJ4	7		0.055	0.977	5.028	-0.179
EMIM-BF_4	+y	4.652	-0.326	3.088	6.664	-0.275	-2.404	0.026	LJ1	3	8	0.481	0.971		
									LJ2	3	8	0.363	0.978	5.020	-0.141
									LJ3	5	6	0.292	0.982	4.741	-0.219
									LJ4	6		0.297	0.982	4.681	-0.175
EMIM-PF_6	-y	5.285	-0.262	3.756	7.232	-0.115	-1.649	0.012	LJ1	7	8	0.036	0.997		
									LJ2	6	9	0.036	0.997	5.338	-0.235
									LJ3	7	8	0.030	0.997	5.311	-0.245
									LJ4	8		0.031	0.997	5.239	-0.234
EMIM-PF_6	+y	5.107	-0.228	3.319	6.681	-0.282	-2.503	0.024	LJ1	5	7	1.033	0.965		
									LJ2	7	8	0.407	0.986	5.475	-0.044
									LJ3	5	6	0.139	0.995	5.409	-0.203
									LJ4	5		0.150	0.995	5.466	-0.271

Table 1: Calculated parameters and fitting constants separated by system (EMIM-BF_4 and EMIM-PF_6) and by direction ($\pm$y) and the four different LJ fits took into account (LJ1-LJ4). $d_{\mathrm{j2m}}(Å)$ and $d_{\mathrm{j2c}}(Å)$ are the critical radii while $E_{vdW}^{d_{\mathrm{j2c}}}(Ha)$, C_{vdW} and χ^2_{vdW} are calculated for each system from Eqs.(5), (7) and (8) respectively. χ^2 and R^2 represent the value of the merit function of unity weights set for the four calculations from Eqs. (12), (14) and (27). $d_0^{num.}$ and $E_0^{num.}$ represent respectively the numerical position and value of the minimum of the energy well. d_0 and E_0 on the contrary represent position and value of the minimum of the energy well recalculated analytically after the fitting procedure. Note that for LJ1 there is no analytically derived d_0 and E_0 but only the m/n coefficients. LJ2 lets the two values vary on a grid around the numerical values. LJ3 values are calculated from Eqs.(19, 20), while LJ4 values come from Eqs.(24, 25).

System	*dir.*	*Fit*	α	β	γ	R^2
EMIM-BF_4	$+y$	LJ3	19.8546	0.1036	0.0238	0.9560
		LJ4	19.9639	0.0985	0.0141	0.9323
EMIM-BF_4	$-y$	LJ3	18.3312	0.1168	-0.0282	0.9843
		LJ4	18.6337	0.1036	-0.0613	0.8199
EMIM-PF_6	$+y$	LJ3	25.2752	0.0989	0.1937	0.8334
		LJ4	25.4356	0.0939	0.1695	0.8077
EMIM-PF_6	$-y$	LJ3	22.3955	0.1254	-0.0618	0.8458
		LJ4	22.8929	0.1087	-0.0958	0.7410

Table 2: Fitting parameters for $A_c(r)$ vs Load from Eqs. (31) and (32).

List of Figures

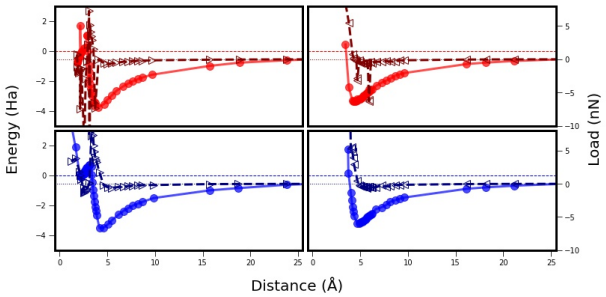

Figure 1: *Ab-initio* interaction energies (left axis, full circles, light colors) and forces between the ions (right axis, open triangles, dark colors) obtained by using second order central differences within the numpy.gradient function. Top row shows calculated data for EMIM-BF_4 (red), whereas the bottom row for EMIM-PF_6 (blue). Data in left ($+y$) and right ($-y$) columns are corresponding to two approaching directions of the anion towards the cation as specified by the orientation of triangles.

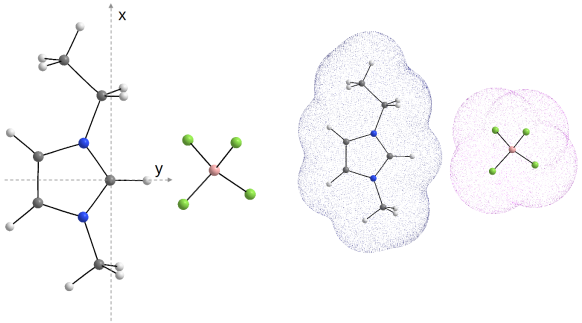

Balls-stick representation of EMIM-BF_4 .

Bader's manifold of EMIM-BF_4 .

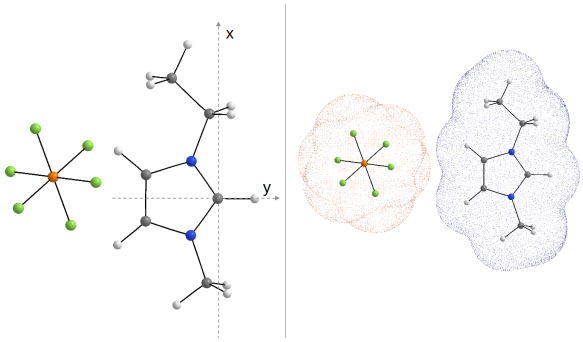

Balls-stick representation of EMIM-PF_6 .

(a) Bader's manifold of EMIM-PF_6 .

Figure 2: The two ionic systems considered in this research: EMIM-BF_4 aligned in the $+y$ direction (top) and EMIM-PF_6 aligned in the opposite $-y$ direction (bottom). The left column shows their ball-stick representation, whereas in the right column the Bader's manifolds of the non-interacting ions in the *separable phase* are given.

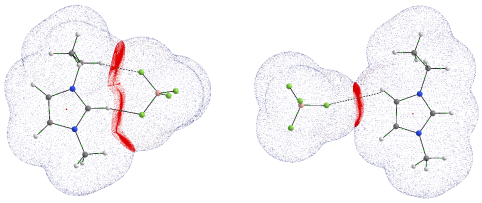

(a) EMIM-BF_4 in the $+y$ direction (left) and the -y direction (right).

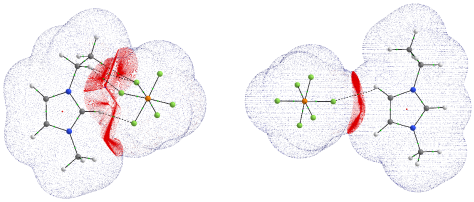

(b) EMIM-PF_6 in the $+y$ direction (left) and the -y direction (right).

Figure 3: Bader analysis of EMIM-BF_4 (top) and EMIM-PF_6 (bottom) for distances between d_{j2m} and d_{j2c} with the two distinguishable Bader manifolds and the area separating the ions (in red). Rows and columns are as in Fig. 1. The anions are approaching the cations following either the $+y$ (left column), or -y direction (right column).

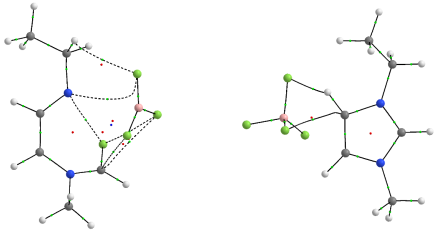

(a) EMIM-BF_4 in the $+y$ direction (left) and the -y direction (right).

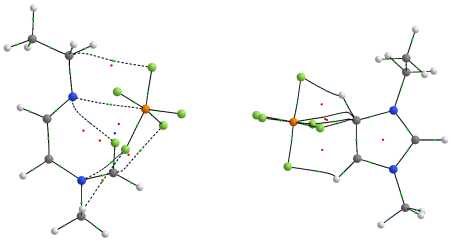

(b) EMIM-PF_6 in the $+y$ direction (left) and the -y direction (right).

Figure 4: Bader analysis of EMIM-BF_4 (top) and EMIM-PF_6 (bottom) for distances below the first transition point d_{j2m} , or in the *indistinguishable phase*. Rows and columns are as in Fig. 1. Small red and green spheres are denoting critical points, see more details in the text. On the left ($+y$ direction) the two ions have completely lost their initial structure, with the imidazolium ring broken and the anion completely distorted. On the right column, corresponding to the -y direction, the global distortion is less pronounced and the two ions are still keeping their initial structures even below d_{j2m} . These differences are also showing up in the charge transfer analyzed in Fig. 5, which features a large charge transfer in the $+y$ direction, while in the -y direction this is almost imperceptible.

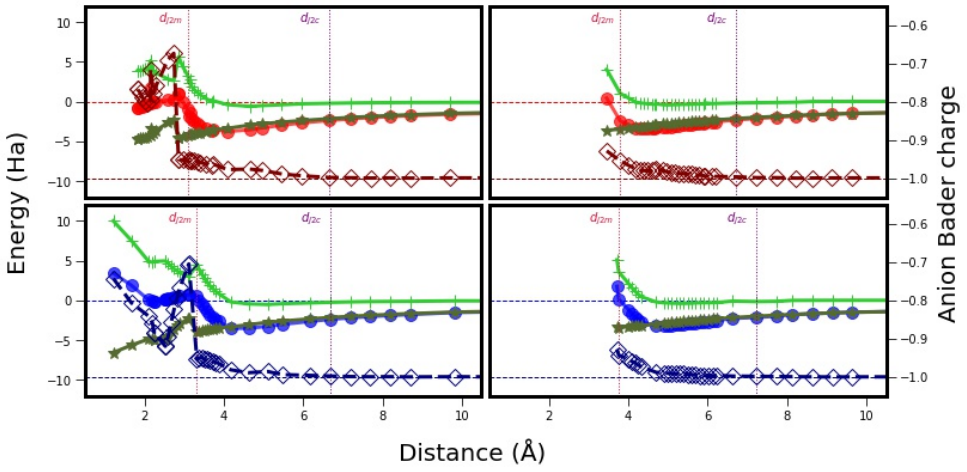

Figure 5: Interaction energies as a function of distance (as in Fig. 1), their Coulomb (dark green stars) and non-Coulomb parts (light green pluses) for EMIM-BF_4 (top panels) and EMIM-PF_6 (bottom panels). Vertical dotted lines are marking the two distances d_{j2m} (red) and d_{j2c} (purple), further details on these distances are given in the text. Anion Bader charges (diamonds) are provided on the right vertical axes. Rows and columns are as in Fig. 1. Left panels correspond to the approach along the $+y$ direction, whereas right panels to the -y direction.

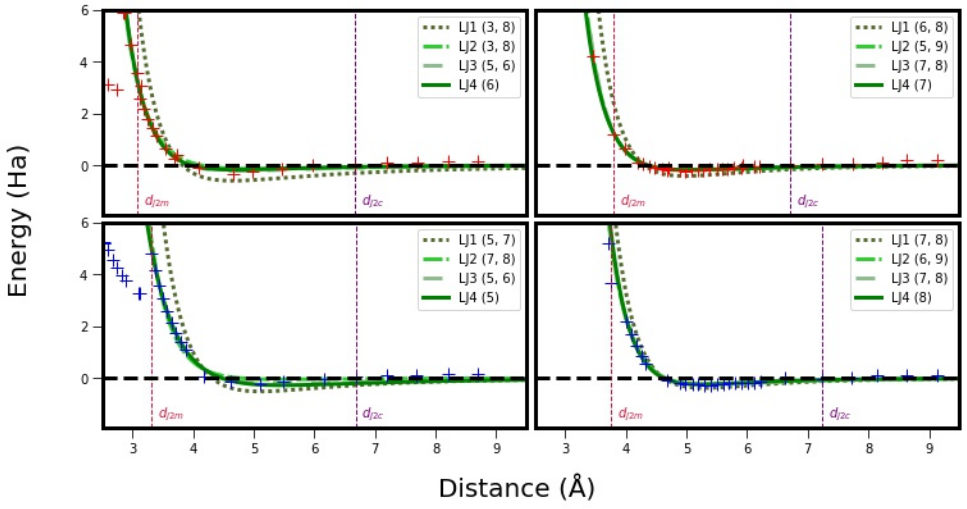

Figure 6: Lennard-Jones fits (green curves) to Energy from Eq. (9). Simulation results are represented by pluses (colors refer to the system, *i.e.* red for EMIM-BF_4 and blue for EMIM-PF_6), while the four LJ fits (recall Sec. 2) are represented with 4 different green lines (dotted, dashed-dotted, dashed and continuous respectively). The exponents of the fits are given in the legend as well in Tab. 1. As in Figs. 1 and 5, the top panel is EMIM-BF_4 while the bottom panel is EMIM-PF_6 . Left/right panels correspond respectively to the approach along the $+y$/-y directions. The vertical lines represent d_{j2m} (red) and d_{j2c} (purple).

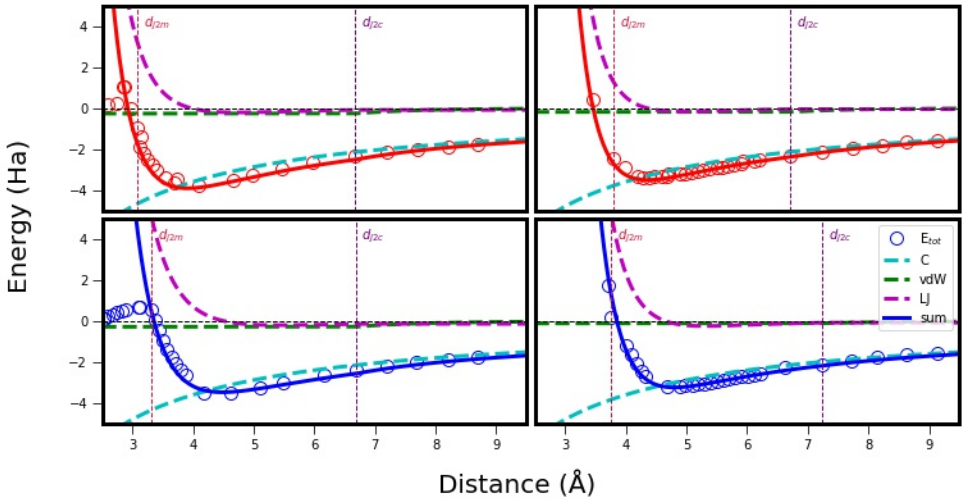

(a) Interaction energies from simulations (open circles) compared to our decomposition (recall Sec. 2). The sum, in blue, of three components (namely the Coulomb component from Eq. (3) in cyan, the vdW component from (5) in green and the better fitting LJ component from either Eq.(10), (13) or (21) in magenta) perfectly matches the simulations results (open circles).

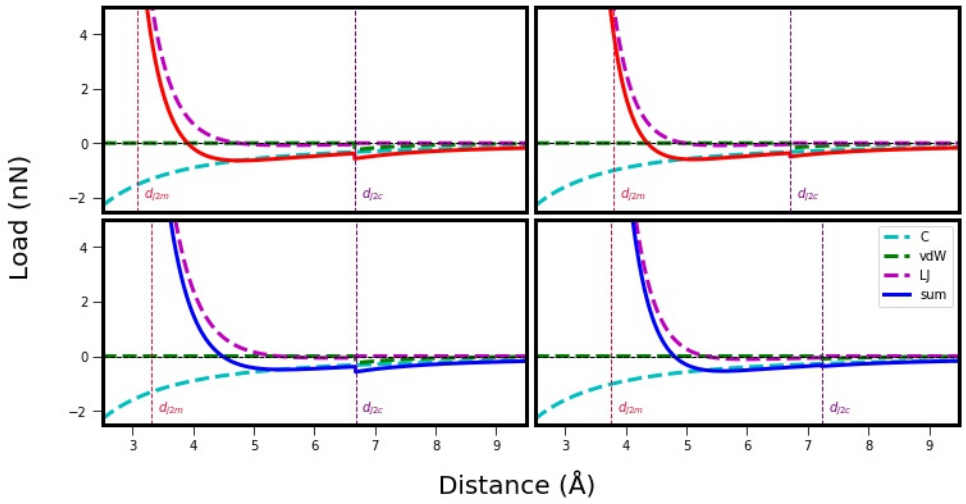

(b) Forces components resulting from our decomposition (recall Sec. 2): Coulomb force from Eq. (4) in cyan, the vdW component from (6) in green and the better fitting LJ component from either Eq.(11), (18) or (26) in magenta.

Figure 7: Interaction energies (top) and forces (bottom) and their components according to our decomposition in Sec. 2. Cyan/dashed-Coulomb component, green/dashed-van der Waals component, purple/dashed-best Lennard-Jones fit (always LJ3), and blue/full-their sum. Top/bottom panels represent results for EMIM-BF_4 /EMIM-PF_6 in red/blue. Left/right panels correspond respectively to the approach along the $+y$/$-y$ directions. The vertical lines represent d_{j2m} (red) and d_{j2c} (purple).

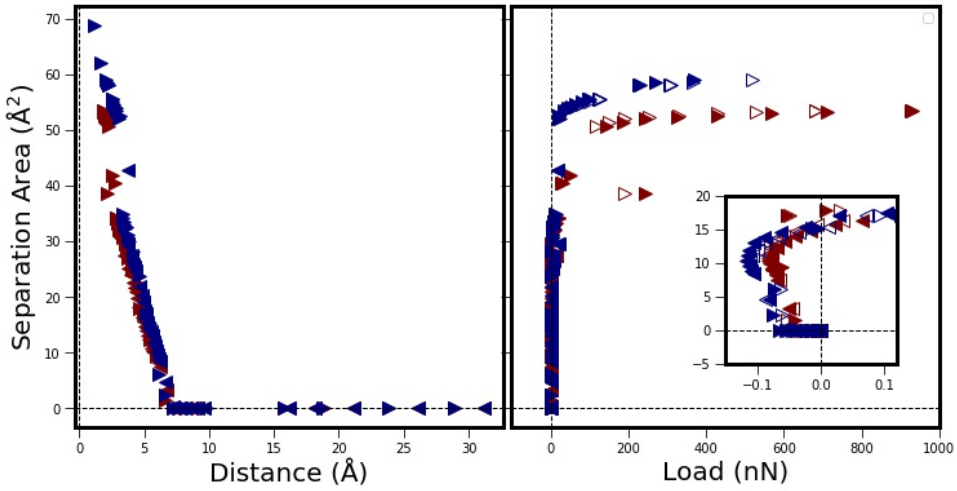

(a) *Ab-initio* calculated separation area between the ions for EMIM-BF_4 (red) and EMIM-PF_6 (blue) as a function of distance (left) and force or load (right). The inset in right panel shows a magnification around the origin.

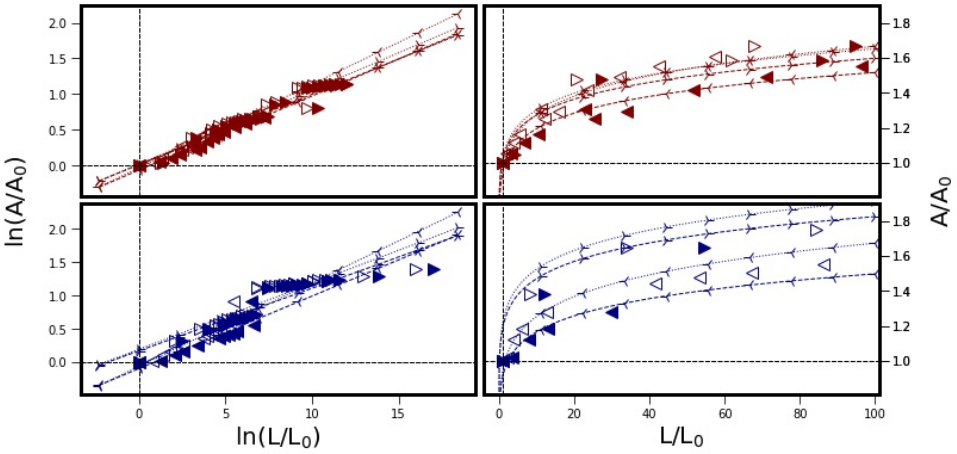

(b) Results of fitting procedure Eq. (31). Numerical results are given in Tab. 2. Left: linear relation between the two logarithms. Right: same relation on a linear scale. Top: EMIM-BF_4 , bottom: EMIM-PF_6 .

Figure 8: Our procedure reveals an universal behavior independent of the system, direction and fitting method. Full/empty triangles denote respectively fitting methods 3 and 4 while the orientation of triangles is in accordance with the direction of the approach along the y-axis.

References

[1] P. Hohenberg, W. Kohn, Inhomogeneous electron gas, Phys. Rev. 136 (3B) (1964) 864–871.

[2] W. Kohn, L. J. Sham, Self-consistent equations including exchange and correlation effects, Phys. Rev. 140 (4A) (1965) 1133–1138.

[3] W. Kohn, Electronic structure of matter – wave functions and density functionals, Nobel Lecture (1999) 213–237.

[4] J. A. Pople, Quantum chemical models, Nobel Lecture (1999) 248–260.

[5] R. M. Martin, Electronic Structure – Basic Theory and Practical Methods, Cambridge University Press, 2020.

[6] R. F. W. Bader, The density in density-functional theory, J. Mol. Struct: THEOCHEM 943 (2010) 2.

[7] R. F. W. Bader, Atoms in Molecules – A Quantum Theory, Oxford University Press, 1994.

[8] R. F. W. Bader, A quantum theory of molecular structure and its applications, Chemical Reviews 91 (5) (1991) 893–928. doi:10.1021/cr00005a013.

[9] R. F. Bader, Atoms in Molecules—a Quantum Theory, Clarendon Press, Oxford, UK, 1990.

[10] M. Wolloch, G. Feldbauer, P. Mohn, J. Redinger, A. Vernes, Ab-initio calculation of the real contact area on the atomic scale, Phys. Rev. B 91 (2015) 195436.

[11] S. Eder, A. Vernes, G. Betz, Methods and numerical aspects of nanoscopic contact area estimation in atomistic tribological simulations, Computer Physics Communications 185 (2014) 217–228.

[12] J.-P. Hansen, I. R. McDonald, Ionic Liquids, Elsevier, 2013. doi:10.1016/b978-0-12-387032-2.00010-6.

[13] Y. Zhou, J. Qu, Ionic liquids as lubricant additives: A review, ACS Applied Materials and Interfaces 9 (4) (2017) 3209–3222. doi:10.1021/acsami.6b12489.

[14] A. E. Somers, P. C. Howlett, D. R. MacFarlane, M. Forsyth, A review of ionic liquid lubricants, Lubricants 1 (1) (2013) 3–21. doi:10.3390/lubricants1010003.

[15] K. N. Marsh, J. A. Boxall, R. Lichtenthaler, Room temperature ionic liquids and their mixtures - A review, Fluid Phase Equilibria 219 (1) (2004) 93–98. doi:10.1016/j.fluid.2004.02.003.

[16] R. L. Vekariya, A review of ionic liquids: Applications towards catalytic organic transformations, Journal of Molecular Liquids 227 (2017) 44. doi:10.1016/j.molliq.2016.11.123.
URL `http://dx.doi.org/10.1016/j.molliq.2016.11.123`

[17] S. Keskin, D. Kayrak-Talay, U. Akman, Ö. Hortaçsu, A review of ionic liquids towards supercritical fluid applications, Journal of Supercritical Fluids 43 (1) (2007) 150–180. doi:10.1016/j.supflu.2007.05.013.

[18] M. Salanne, Simulations of room temperature ionic liquids: From polarizable to coarse-grained force fields, Physical Chemistry Chemical Physics 17 (22) (2015) 14270–14279. arXiv:1505.07860, doi:10.1039/c4cp05550k.
URL `http://dx.doi.org/10.1039/C4CP05550K`

[19] E. Choi, J. G. McDaniel, J. R. Schmidt, A. Yethiraj, First-principles, physically motivated force field for the ionic liquid [BMIM][BF4], Journal of Physical Chemistry Letters 5 (15) (2014) 2670–2674. doi:10.1021/jz5010945.

[20] K. Karu, A. Ruzanov, H. Ers, V. Ivaništšev, I. Lage-Estebanez, J. M. de la Vega, Predictions of physicochemical properties of ionic liquids with DFT, Computation 4 (3) (2016) 1–14. doi:10.3390/computation4030025.

[21] W. Zhong, D. Tomanek, First-Principles Theory of Atomic-Scale Friction, Physical Review Letters 64 (25) (1990) 3054–3057.

[22] R. Neitola, T. A. Pakkanen, Ab initio studies on the atomic-scale origin of friction between hydrocarbon layers, Chemical Physics 299 (1) (2004) 47–56. doi:10.1016/j.chemphys.2003.11.037.

[23] L. F. Wang, T. B. Ma, Y. Z. Hu, H. Wang, T. M. Shao, Ab initio study of the friction mechanism of fluorographene and graphane, Journal of Physical Chemistry C 117 (24) (2013) 12520–12525. doi:10.1021/jp401097a.

[24] M. W. Schmidt, K. K. Baldridge, J. A. Boatz, S. T. Elbert, M. S. Gordon, J. H. Jensen, S. Koseki, N. Matsunaga, K. A. Nguyen, S. Su, T. L. Windus, M. Dupuis, J. A. Montgomery Jr, General atomic and molecular electronic structure system, Journal of Computational Chemistry 14 (11) (1993) 1347–1363. doi:10.1002/jcc.540141112.
URL https://onlinelibrary.wiley.com/doi/abs/10.1002/jcc.540141112

[25] M. Gordon, M. Schmidt, Advances in electronic structure theory: Gamess a decade later, in: Theory and Applications of Computational Chemistry: the first forty years, Elsevier, Amsterdam, 2005, pp. 1167–1189, editors: C.E. Dykstra, G. Frenking, K.S. Kim and G.E. Scuseria.

[26] T. Clark, J. Chandrasekhar, G. W. Spitznagel, P. V. R. Schleyer, Efficient diffuse function-augmented basis sets for anion calculations. iii. the 3-21+g basis set for first-row elements, li-f, J. Comput. Chem. 4 (1983) 294–301. doi:10.1002/jcc.540040303.

[27] R. Krishnan, J. S. Binkley, R. Seeger, J. A. Pople, Self-consistent molecular orbital methods. xx. a basis set for correlated wave functions, J. Chem. Phys. 72 (1980) 650–654. doi:10.1063/1.438955.

[28] A. D. McLean, G. S. Chandler, Contracted gaussian basis sets for molecular calculations. i. second row atoms, z=11-18, J. Chem. Phys. 72 (1980) 5639–5648. doi:10.1063/1.438980.

[29] G. W. Spitznagel, T. Clark, P. v. R. Schleyer, W. J. Hehre, An evaluation of the performance of diffuse function-augmented basis sets for second row elements, na-cl, J. Comput. Chem. 8 (1987) 1109–1116. doi:10.1002/jcc.540080807.

[30] A. D. Becke, Density-functional thermochemistry. iii. the role of exact exchange, The Journal of Chemical Physics 98 (7) (1993) 5648–5652. doi:10.1063/1.464913.

[31] C. Lee, W. Yang, R. G. Parr, Development of the colle-salvetti correlation-energy formula into a functional of the electron density, Phys. Rev. B 37 (1988) 785–789. doi:10.1103/PhysRevB.37.785.
URL https://link.aps.org/doi/10.1103/PhysRevB.37.785

[32] S. H. Vosko, L. Wilk, M. Nusair, Accurate spin-dependent electron liquid correlation energies for local spin density calculations: a critical analysis, Canadian Journal of Physics 58 (8) (1980) 1200–1211. doi:10.1139/p80-159.

[33] P. J. Stephens, F. J. Devlin, C. F. Chabalowski, M. J. Frisch, Ab initio calculation of vibrational absorption and circular dichroism spectra using density functional force fields, The Journal of Physical Chemistry 98 (45) (1994) 11623–11627. doi:10.1021/j100096a001.

[34] S. Grimme, S. Ehrlich, L. Goerigk, Effect of the damping function in dispersion corrected density functional theory, Journal of Computational Chemistry 32 (7) (2011) 1456–1465. arXiv:https://onlinelibrary.wiley.com/doi/pdf/10.1002/jcc.21759, doi:10.1002/jcc.21759.
URL https://onlinelibrary.wiley.com/doi/abs/10.1002/jcc.21759

[35] R. F. Bader, M. T. Carroll, J. R. Cheeseman, C. Chang, Properties of atoms in molecules: atomic volumes, Journal of the American Chemical Society 109 (26) (1987) 7968–7979.

[36] T. A. Keith, Aimall, aim.tkgristmill.com (1997-2019).

[37] Django, https://djangoproject.com (2019).

[38] A. C. F. Mendonca, P. Malfreyt, A. A. H. Padua, Interactions and ordering of ionic liquids at a metal surface, J. Chem. Theory Comput. 8 (2012) 3348–3355.

[39] K. Gkagkas, V. Ponnuchamy, M. Dašić, I. Stanković, Molecular dynamics investigation of a model ionic liquid lubricant for automotive applications, Tribology International 113 (2017) 83–91, 43rd Leeds - Lyon Symposium on Tribology 2016. doi:https://doi.org/10.1016/j.triboint.2016.12.017.
URL https://www.sciencedirect.com/science/article/pii/S0301679X1630490X

[40] M. Dašić, I. Stanković, K. Gkagkas, Molecular dynamics investigation of the influence of the shape of the cation on the structure and lubrication properties of ionic liquids, Phys. Chem. Chem. Phys. 21 (2019) 4375–4386. doi:10.1039/C8CP07364C.
URL http://dx.doi.org/10.1039/C8CP07364C

[41] M. Salanne, L. J. Siqueira, A. P. Seitsonen, P. A. Madden, B. Kirchner, From molten salts to room temperature ionic liquids: Simulation studies on chloroaluminate systems, Faraday Discussions 154 (2012) 171–188. arXiv:1303.3878, doi:10.1039/c1fd00053e.

[42] C. Merlet, M. Salanne, B. Rotenberg, New coarse-grained models of imidazolium ionic liquids for bulk and interfacial molecular simulations, Journal of Physical Chemistry C 116 (14) (2012) 7687–7693. doi:10.1021/jp3008877.

[43] K. L. Johnson, K. Kendall, A. D. Roberts, Surface energy and the contact of elastic solids, Proceedings of the Royal Society of London. A. Mathematical and Physical Sciences 324 (1558) (1971) 301–313. doi:10.1098/rspa.1971.0141.

[44] K. L. Johnson, Contact Mechanics, Cambridge University Press, 1987.

[45] R. W. Carpick, N. Agrait, D. F. Ogletree, M. Salmeron, Variation of the interfacial shear strength and adhesion of a nanometer-sized contact, Langmuir 12 (1996) 3334–3340.

[46] A. Vernes, S. Eder, G. Vorlaufer, G. Betz, On the three-term kinetic friction law in nanotribological systems, Faraday Discuss 156 (2012) 173–196.

[47] S. J. Eder, G. Feldbauer, D. Bianchi, U. Cihak-Bayr, G. Betz, A. Vernes, Applicability of macroscopic wear and friction laws on the atomic length scale, Phys. Rev. Letts. 115 (2015) 025502.